Magnetic Resonance Imaging 76 (2021) 1–7

Contents lists available at ScienceDirect

Magnetic Resonance Imaging

journal homepage: www.elsevier.com/locate/mri

Technical Note

Ficoll as testing material for diffusion weighted imaging-quality assurance phantoms

Andrea Barucci [a,*,1], Alessandra Flori [b,1], Roberto Carpi [c], Daniele De Marchi [d], Marco Esposito [c], Luca Menichetti [e], Roberto Pini [a], Fulvio Ratto [a], Giacomo Belli [f], Francesco Piazza [g]

[a] "Nello Carrara" Institute of Applied Physics, CNR Florence Research Area, Via Madonna del Piano 10, 50019 Sesto Fiorentino, FI, Italy
[b] Bioengineering and clinical engineering unit, Fondazione CNR/Regione Toscana G. Monasterio, Via G. Moruzzi 1, 56124 Pisa, Italy
[c] USL Toscana Centro, Piazza Santa Maria Nuova 1, 50121 Firenze, Italy
[d] MRI unit, Fondazione CNR/Regione Toscana G. Monasterio, Via G. Moruzzi 1, 56124 Pisa, Italy
[e] Institute of Clinical Physiology, CNR, Via G. Moruzzi 1, 56124 Pisa, Italy
[f] Health Physics Unit, AOU Careggi, Largo Brambilla 3, 50134 Firenze, Italy
[g] Université d'Orléans and Centre de Biophysique Moléculaire (CBM), CNRS UPR 4301, rue Charles Sadron, 45071 Orléans, France

ARTICLE INFO

Keywords:
Ficoll
Phantoms
Diffusion weighted imaging
Quality assurance
Magnetic resonance imaging

ABSTRACT

Purpose: The aim of this work is to test the use of aqueous solutions of Ficoll®**, a highly branched polymer displaying crowding properties, to build a phantom suitable for Diffusion Weighted Imaging (DWI) in Magnetic Resonance Imaging (MRI).

Methods: We developed a test object made of a cylindrical plastic container with a precise geometrical arrangement suitable for measuring several samples at the same time. The container was designed to host single vials with variable geometry and number, and to fit inside common commercial head coils for MRI scanners.
In our experiments, vials were filled with 8 aqueous solutions of Ficoll 70 and Ficoll 400 spanning a range of polymer concentration from 5 to 30% by weight. Vials containing ultra-pure water were also used as reference. Experiments were performed on both 1.5 and 3 T clinical scanners (GE, Philips and Siemens), under the conditions of a standard clinical examination.

Results: The geometry of the phantom provided reduced imaging artifacts, especially image distortions at magnetic interfaces. We found that the Apparent Diffusion Coefficient (ADC) varied in the range of 0.00125–0.00223 mm^2/s and decreased with Ficoll concentration. ADC vs Ficoll concentration exhibited a linear trend. Results were consistent over time and among different MRI clinical scanners, showing an average variability of 3% at 1.5 T and of 7.5% at 3 T. Moreover, no substantial difference was found between Ficoll 70 and 400. By varying Ficoll concentration, ADC can be modulated to approach tissue-mimicking values. Preliminary results for relaxation measurements proved that both T_1 and T_2 decreased with Ficoll concentration in the ranges 1.3–2.4 *s* and 150–800 *ms* respectively.

Conclusions: In this work, we propose a 3D phantom design based on the widespread crowding agent Ficoll, which is suitable for DWI quality assurance purposes in MRI acquisitions. Aqueous Ficoll solutions provide good performance in terms of stability, ease of preparation, and safety.

1. Introduction

Magnetic Resonance Imaging (MRI) enables anatomic mapping of quantitative tissue parameters, such as relaxation times T_1 (spin-lattice) and T_2 (spin-spin), and the Apparent Diffusion Coefficient (ADC). By accounting for the diffusion-related attenuation of MRI signal intensity, ADC positively correlates with tissue cellularity [1], and so may become a useful metric for tumor characterization. Moreover, ADC maps help assess early response to oncological treatments [1]. Quantitative MRI methods aimed at estimating tissue parameters are usually validated using phantoms [2,3] containing separate vials of chemically-doped aqueous solutions designed to mimic different tissue parameters, such

* Corresponding author.
E-mail address: a.barucci@ifac.cnr.it (A. Barucci).
[1] These authors contribute equally to this work and must be considered both as first author.

https://doi.org/10.1016/j.mri.2020.11.001
Received 15 April 2020; Received in revised form 3 November 2020; Accepted 3 November 2020
Available online 6 November 2020
0730-725X/© 2020 Elsevier Inc. All rights reserved.

as relaxation times T_1 and T_2, and diffusion coefficients [4,5]. These phantoms are suitable for Quality Assurance (QA) purposes, but also for testing instrument performance and imaging sequences. Among the ideal characteristics, the material used for MRI tissue-mimicking phantoms should provide T_1 and T_2 values comparable to those of human tissues. This is often not the case for phantoms consisting of aqueous solutions [2]. Gel phantoms, on the other hand, have the disadvantages of being unstable over time and suffering from poor reproducibility [3,5]. Other phantoms such as ice-water phantoms [6–10] and polyvinylpyrrolidone (PVP) phantoms [9,11] have shown good performance in single and multicenter trials, and are robust against changing MRI sequence or hardware design and temperature fluctuations [6,7]. A review on quantitative MRI phantoms was compiled by Keenan et al. [9,12]. The need for standardization protocols and for validated quantitative imaging biomarkers is witnessed, for instance, by the work of the Quantitative Imaging Biomarkers Alliance (QIBA, http://qibawiki.rsna.org/).

In this work, we develop and test an MRI phantom for ADC QA protocols with tissue-mimicking parameters, based on aqueous solutions of Ficoll® [13]. Ficoll is a highly branched polymer made of sucrose monomers cross-linked by epichlorohydrin molecules. Due to its abundance of hydroxyl groups, Ficoll is highly hydrophilic and readily dissolves in water to form hydrogels up to densities as high as 50% by weight. From a soft-matter standpoint, Ficoll takes the form of spherical porous particles, featuring bound-water layers in and outside, displaying signatures of softness and attractive interactions, and forming stable suspensions that comprise monomers and clusters at high concentrations [14]. Typical hydrodynamic radii are about 5 to10 nm, for molecular weights of (approximately) 70 (Ficoll 70) and 400 kDA (Ficoll 400) [15]. Over the past decade, Ficoll has become a popular model to mimic macromolecular crowding (MMC) conditions, and to investigate the stability [16,17], activity [18,19] and diffusion [20,21] of biomolecules in a non-ideal medium, by roughly reproducing the fraction of excluded volume in the cytoplasm, where 30 to 40% of the available space is occupied by all sorts of small and large molecules, membrane-bound organelles and cytoskeletal structures [22]. In addition, Ficoll has been investigated for applications in blood preservation [23] and renal filtration [24]. However, to the best of our knowledge, its use as an MRI phantom has never been reported before.

The aim of this study was to investigate the use of Ficoll as a functional material for MRI phantoms, suitable for DWI QA protocols. To this purpose, we assessed the dependence of ADC on the concentration of Ficoll 70 and 400 in aqueous solution.

2. Materials and methods

2.1. Phantom geometry

2.1.1. Phantom container

The phantom was constructed as a cylindrical plastic container made of Plexiglas (Fig. 1a,b) with height and diameter of 16 cm. Dimensions were chosen to allow its use in all the head coils commercially available for clinical scanners with good filling factor. The interior of the container can be accessed through a lid that was designed to ensure hermetic sealing and to allow the expulsion of air bubbles.

The container potentially holds multiple Plexiglas tier dividers (Fig. 1a,b) [25]. In our work, we used a configuration with 2 tier dividers, each accommodating 9 slots for 8-mL vials along their circumference, plus another slot in their center preferably serving as an extra reference typically filled with deionized water.

Vials are commercially available plastic containers with a fixed volume of 8 mL and a hermetic cap. Each vial can be filled with the solution of interest for the experiment, and can be replaced at any time with minimal effort.

The geometric layout of the vials inside the plastic container was chosen to minimize the incidence of artifacts like image distortions.

2.2. Phantom preparation

We prepared 16 vials containing Ficoll 70 or 400 in ultrapure (MilliQ) water at the concentrations of 5, 10, 12.5, 15, 17.5, 20, 25 and 30% by weight.

Ficoll dissolution was achieved by magnetic stirring at 760–800 rpm at room temperature for 40 min – 1 h, depending on the concentration.

Until 30% by weight, Ficoll solutions were in a fluid state, and did not form a gel. At higher concentrations, the viscosity progressively increased. All solutions appeared to be transparent, with a slight tendency to turn yellow with the concentration of Ficoll. All samples were also supplemented with 0.0013% sodium-azide as a preservative, and thoroughly vortexed prior to loading into their vials. Each vial was filled to its brim, in order to minimize the presence of air, secured with laboratory film (Parafilm® M) and inserted in a dedicated slot in the Plexiglas container.

In our experiments, the top tier accommodated Ficoll 70 vials, while the bottom one Ficoll 400. Vials closer to the centre of each tier were filled with ultrapure (MilliQ) water as reference. The phantom container was finally filled with deionized water, which was not supplemented with sodium-azide and was renewed before each measurement session.

2.3. Measurements

2.3.1. MRI acquisition: scanner and sequences

Measurements were performed at different magnetic field strengths and using different clinical scanners (1.5 T Signa Excite, GE; 3 T Signa HDxT, GE; 1.5 T Ingenia, Philips; 3 T Ingenia Philips; 1.5 T Magnetom Aera Siemens).

For each measurement, the phantom was kept in the magnet room for at least 5 h for thermalizing before starting the acquisitions. Following the recommendations of report n. 12 (2016) of Italian Association of Medical Physics (AIFM) [26], the temperature of the phantom

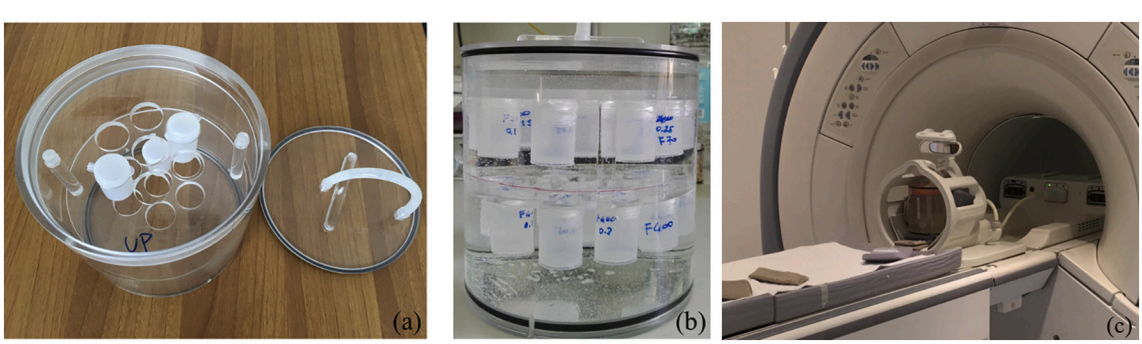

Fig. 1. Phantom images showing an example of the geometrical arrangement of the vials inside the plastic container. Panel b) shows the case with 18 8-mL vials used in the experiments described in this work. Panel c) shows the phantom inside a head coil of a 3 T clinical scanner.

was checked at the beginning and at the end of each measurement session, giving values of 22 ± 1 °C, in agreement with the temperature of the thermalized room (22 ± 2 °C).

All cylinders were always imaged in a single measurement session without repositioning. The phantom was placed upright at the magnet isocenter, inside a head coil (Fig. 1c). Coronal slices were acquired using sequences with the parameters reported in Table 1. For all sequences, volume shimming was applied, while co-registration was not. For diffusion measurements, we selected the following *b*-values: 0, 250, 500, 750, 1000, 1250, 1500, 1750, 2000, 2250, 2500 and 3000 s/mm^2.

In order to understand the reliability of the data for standardization purposes, measurements were repeated 4 times over a time span of about 1 year, and 1 additional time after 3 years.

Preliminary measurements of the relaxation times (T_1 and T_2) were also performed at 1.5 T (Signa Excite, GE) and 3 T (Signa HDxT, GE). Relevant acquisition details are reported in Table 2.

An FSE sequence was tested in one scanner, in order to evaluate its performance with respect to the more clinically popular EPI sequence. Results were similar, thus suggesting that the EPI sequence is reliable for these measurement settings. Slice width and matrix size varied according to the different scanner protocols and constraints. The number of values for Echo-time (TE) and Inversion-time (TI) were affected by the available options, and the values were chosen to cover the best range to retrieve T_1 and T_2, while keeping in mind that the phantom contained different samples, and so required careful trade-offs.

2.4. Post-processing

2.4.1. SNR evaluation on DWI images

To provide a semi-quantitative evaluation of the image quality, we measured the SNR for the different vials containing different Ficoll solutions at varying b-values. The SNR over each sample was calculated by taking into account the Rayleigh noise model [27] and using the following equation:

$$SNR = \frac{S_{ROI}}{\sqrt{\frac{2}{4-\pi}}\sigma_{noise}} \quad (1)$$

where S_{ROI} is the mean value of the MRI signal in a circular region of interest (ROI) at the center of each vial, and σ_{noise} is the standard deviation of the noise calculated over a ROI of the same size in the air outside the DWI phantom. Representative values obtained at 1.5 and 3 T as a function of *b*-value for all samples are reported in Supplementary material (SM, Fig. S3).

2.4.2. ADC estimation

For each vial, the logarithm of the signal intensity averaged over a ROI of ~180 pixels was plotted as a function of *b*-value. Then, the ADC was calculated as the slope of the regression line according to:

$$ln(S) = -b^*ADC + ln(S_0) \quad (2)$$

where S is signal intensity (a.u.) and S_0 is the value obtained for $b = 0$. The fit was performed over the linear portion of the plot [28]. Following QIBA recommendations, ADC was evaluated at varying *b*-values, and the maximum limit *b*-value = 1750 s/mm^2 was chosen in order for the fit of ADC to remain within 5% of bias.

The coefficient of variation (CV = standard deviation/mean value, in percentage) was calculated over the different acquisition sessions and taken as a surrogate index of measurement reproducibility.

The dependence of ADC on Ficoll concentration was also expressed in molar terms by taking into account the different molecular weights of Ficoll 70 (342.3 g/mol) and Ficoll 400 (432.8 g/mol).

2.4.3. T1 and T2 measurements

For T_1 and T_2 estimation, average signals from circular ROIs corresponding to the various vials were extracted with ImageJ [29] and reported as a function of TE for T_2, and of TI for T_1. T_1 and T_2 values were estimated in Matlab (The Mathwork Inc.) by fitting the processed data according to the general equations:

$$ln(M) = ln(M_0) - TE/T_2 \quad (3)$$

$$M = M_0{}^*(1–2^*exp(-TI/T_1)) \quad (4)$$

where M is the magnetization signal and M_0 is the equilibrium magnetization. Results were evaluated in terms of the relaxation rates $R_{1,2}$, defined as the inverse of the respective relaxation times (i.e. $R_{1,2} = 1/T_{1,2}$). Finally, by performing a linear fit of the regression line $R_{1,2}$ vs molar Ficoll concentration, we extrapolated the relaxivities for both Ficoll 70 and 400.

3. Results

Representative images recorded at 1.5 T are shown in Fig. 2, panels b and c. A qualitative analysis of DWI images revealed modest image distortions. An example of a comparison of DWI images of the phantom containing Ficoll 70 at different concentrations, acquired at 1.5 T using EPI and FSE sequences, is shown in Fig. S1 of SM. In parallel, examples of representative DWI images obtained for Ficoll 400 at 3 T using the clinical scanner from Vendor "A" are given in Fig. S2 of SM. As expected, major image distortions were observed for the EPI protocol as compared to the FSE sequence. EPI sequences, by being faster and more robust against motion artifacts, are the gold standard protocol for DWI exams in the clinical practice. However, EPI protocols are prone to local image distortions caused by magnetic interfaces or eddy currents [30]. In our case, as shown in Fig. S1, geometrical distortions were already present at $b = 0$, thus suggesting that the effect of eddy currents induced by diffusion gradients is negligible with respect to the intrinsic deformations of the EPI sequence.

As expected, the SNR substantially decreased with increasing *b*-value. The image quality deteriorates at *b*-values higher than 1750 s/mm^2. For instance, an SNR below 15 was recorded in this region for images acquired at 3 T (see Fig. S3 in SM). The same general trend was observed across all different concentrations, and for both Ficoll 70 and 400, at both 1.5 and 3 T.

A qualitative analysis of the diffusion measurements revealed a linear trend of the logarithm of signal intensity vs. *b*-value for both Ficoll 70 and 400 at different concentrations, up to $b = 2500$ s/mm^2 (Fig. S4 of SM). For $b = 3000$ s/mm^2, a reduced signal attenuation was observed, especially at lower polymer concentrations (Fig. S4 of SM).

However, in order to take into account the SNR reduction and the

Table 1
sequences selected for MRI studies with aqueous solutions of Ficoll 70 and 400 on different scanners and magnetic fields. EPI = Echo Planar Imaging; FSE = Fast Spin Echo. The names of the vendors were omitted in the Table.

Magnetic field	Sequence	Field of view (cm^2)	Slice thickness (mm)	Averages	Matrix size	Repetition time (s)	Echo time (ms)
3 T A	EPI	24 × 24	3	1	128 × 128	8	108
1.5 T A	EPI	24 × 24	5	2	96 × 128	8	90.4
1.5 T B	FSE	23 × 23	5	1	144 × 90	8	127.3
3 T B	EPI	19 × 19	10	1	128 × 128	8	96
1.5C	EPI	19 × 19	10	1–4 (depending on b)	128 × 102	8	109

Table 2
sequences and parameters selected on the different scanners and magnetic fields. FSE = Fast Spin Echo; SE = Spin Echo; IR = Inversion Recovery. The number of values for TE and TI were limited by the available options, and the values were chosen to cover a range suitable to simultaneously measure T_1 and T_2 across the different concentrations of Ficoll.

	Magnetic field	Sequence	Field of view (cm^2)	Slice thickness (*mm*)	Averages	Matrix size	Repetition time (*s*)	Echo time (*ms*)	Inversion time (*ms*)
T_2	3 T	FSE	24 × 24	3	1	256 × 224	2.5	6.6, 25, 45, 85, 105, 125, 155	–
	1.5 T	SE	24 × 24	5	0.5	192 × 128	8	8, 25, 45, 85, 105, 125, 155, 205	–
T_1	3 T	IR	24 × 24	3	1	192 × 192	8	7.3	100, 300, 500, 700, 900, 1100, 1300, 1500, 1700, 2100, 2500
	1.5 T	IR	24 × 24	5	0.5	192 × 128	8	10	100, 500, 900, 1300, 1700, 2100, 2300

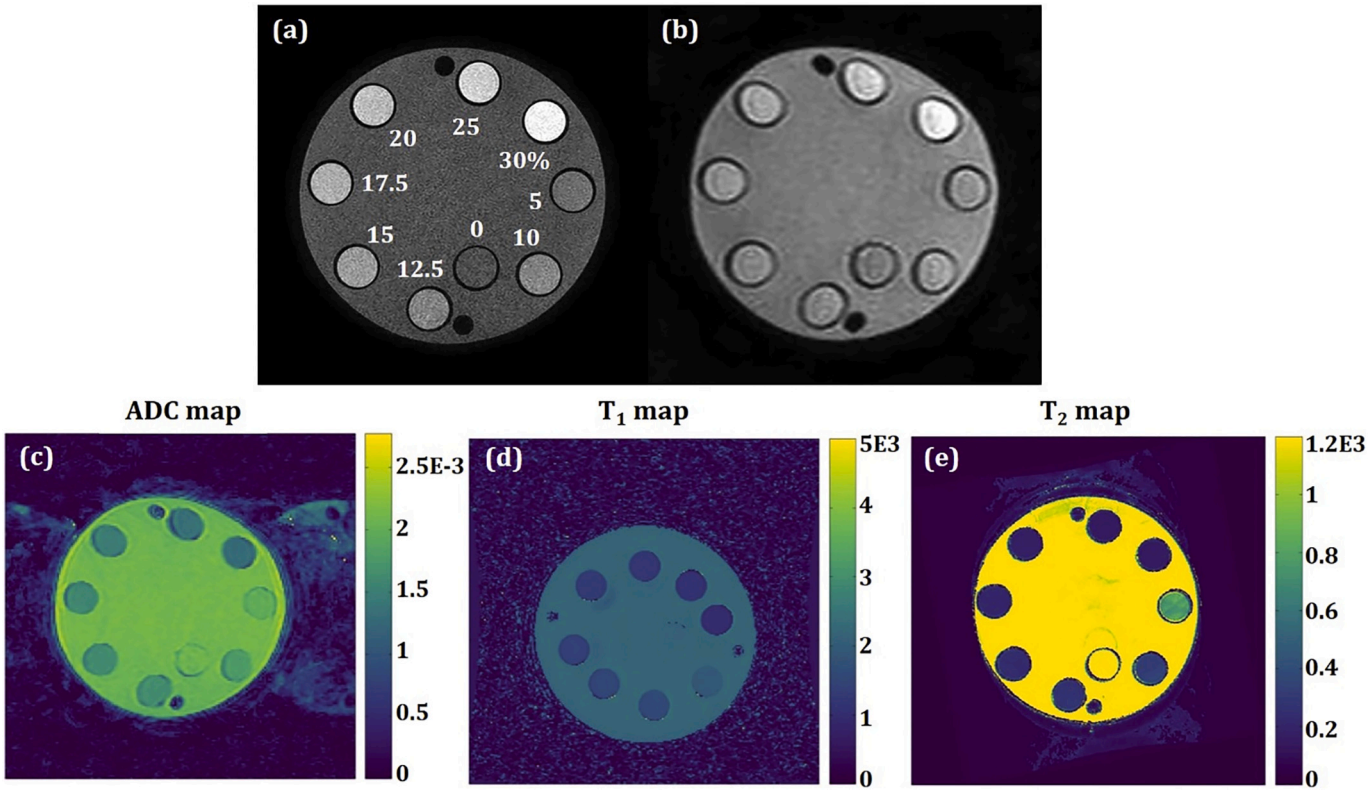

Fig. 2. Panel a) T_1-weighted image labelled with the concentration of Ficoll in each vial. Panel b) shows an example of a DWI image for b = 1000 s/mm^2 and acquired at 1.5 T. Panel c) is an ADC map at 1.5 T. Panel d) shows a T_1 map at 1.5 T. Panel e) is a T_2 map instead. For panel c), the scale is reported in mm^2/s. In panels d) and e), it is reported in ms.

noise floor effect emerging when noise is evaluated from background signal for magnitude images (see Fig. S3 in SM), ADC values were estimated by considering *b*-values until 1750 s/mm^2 (see Fig.S5 of SM).The range of ADC values detected for Ficoll 70 and 400 at 1.5 and 3 T was quite limited and fell in the range 0.00125–0.00223 mm^2/s with an approximately linear decrease with Ficoll concentration (Fig. 3).

The ADC values obtained with Ficoll 70 and 400 were comparable over all studied concentrations, when reported in terms of weight percentage of Ficoll in water. Moreover, the same trend was detected at both 1.5 and 3 T (Fig. 3). No difference was found between the ADC values retrieved from the FSE and EPI acquisition sequences. In turn, when expressed in terms of molar concentration, ADC values were slightly different. By looking at the slope of the regression line of ADC as a function of molar concentration, we found that the measured values were about 20% higher for Ficoll 400 as compared to Ficoll 70. Results are shown in the lower panel of Fig. 3.

The ADC values measured with different MRI scanners were in agreement with each other with a maximum CV of 12%, thus suggesting the consistency of our phantom for multi-scanner measurements.

Results were stable over time as well, and displayed an average CV of 3% at 1.5 T and of 7.5% at 3 T over the different concentrations, thus pointing to a good reproducibility of our measurements. No aging effect of Ficoll was detected across the different experimental sessions either.

From preliminary measurements of relaxation times performed at 1.5 and 3 T, we detected T_1 and T_2 values in the range 1.3–2.4 *s* and 150–800 *ms*, respectively, with an average CV of 7% for the different concentrations at 3 T. In particular, we found a linear increase of $R_{1,2}$ with Ficoll molarity at both field strengths (Fig. 4). Regarding R_1, the relaxation rates were basically converging for Ficoll 70 and 400, and we did not find any dependence on the magnetic field strength (Fig. 4a, b). For R_2, a similar increasing trend was observed for Ficoll 70 and 400 at different magnetic field strengths. However, the values of R_2 for Ficoll 70 at higher concentrations were about 40% lower at 1.5 T than at 3 T (Fig. 4c, d).

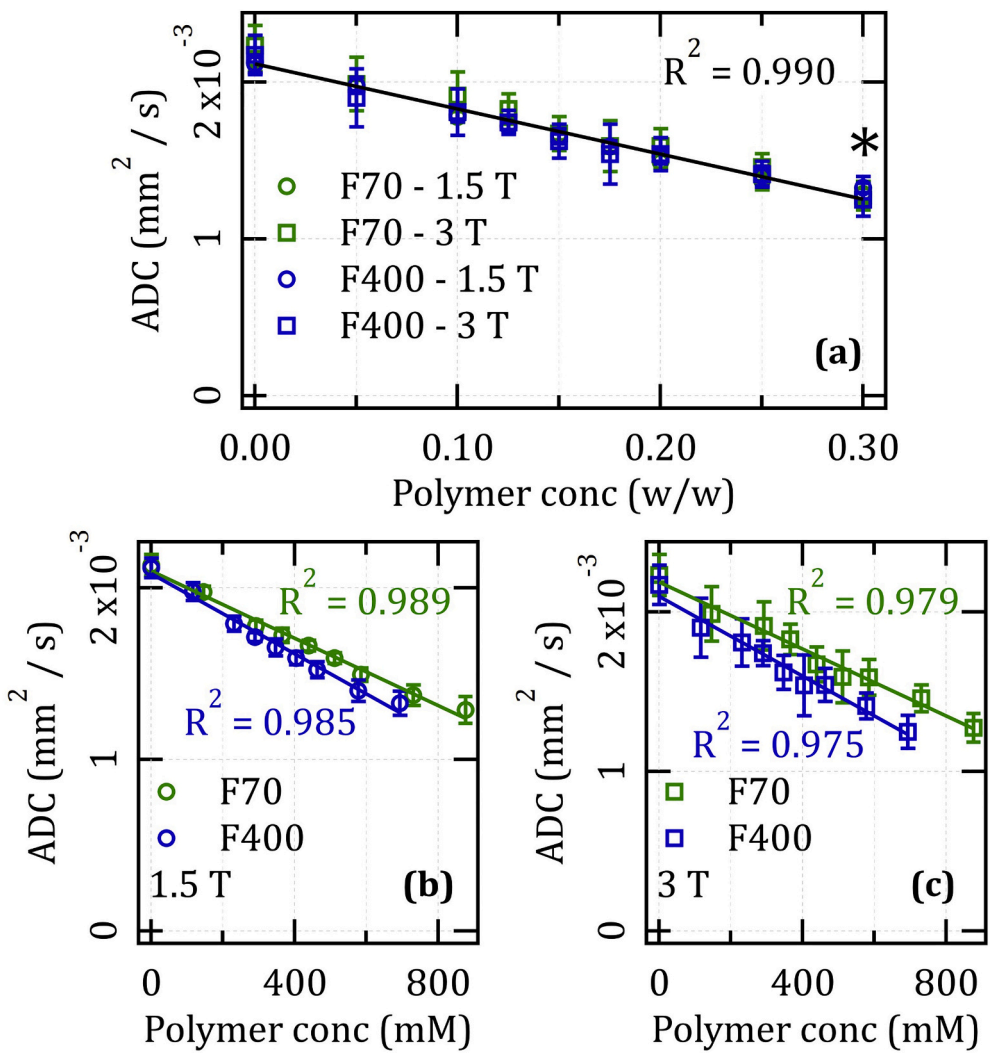

Fig. 3. ADC value vs. Ficoll concentration expressed as weight percent and measured at 1.5 and 3 T (a) or as molarity and probed at 1.5 (b) and 3 T (c), by using different MRI scanners. Error bars indicate the standard deviation of the measurement sessions performed using different clinical scanners, as described in the Materials and methods section. An asterisk in the upper panel indicates that the 30% sample lacked one measurement session. The linear regression returned ADC = $-2.9{\cdot}10^{-3}$ mm^2/s · conc $+2.1{\cdot}10^{-3}$ mm^2/s for the data in panel a), ADC = $-9.83{\cdot}10^{-7}$ mm^2/(s·mM) · conc $+2.10{\cdot}10^{-3}$ mm^2/s for Ficoll 70 and ADC = $-1.17{\cdot}10^{-6}$ mm^2/(s·mM) · conc $+2.08{\cdot}10^{-3}$ mm^2/s for Ficoll 400 in panel b), and ADC = $-1.05{\cdot}10^{-6}$ mm^2/(s·mM) · conc $+2.19{\cdot}10^{-3}$ mm^2/s for Ficoll 70 and ADC = $-1.25{\cdot}10^{-6}$ mm^2/(s·mM) · conc $+2.10{\cdot}10^{-3}$ mm^2/s for Ficoll 400 in panel c).

4. Discussion

In order to reliably test Ficoll polymers as candidates in QA DWI applications, we designed a dedicated phantom hosting as many as 18 different vials and providing for a geometry that minimized imaging artifacts like distortions at magnetic interfaces. Moreover, the phantom proved to be stable, robust, versatile, inexpensive, and easy and safe to fabricate and handle.

The linear decrease of ADC with concentration found in this study (Fig. 3) was previously reported for agar gel solutions [31], and it was attributed to an increase in the hydrogen bonding interactions restricting the diffusivity of water. A similar hypothesis may be drawn for Ficoll, consistent with the work by Palit et al. [14] and Aouissi et al. [32], for types 70 and 400, respectively. In this study, the diffusion signal reported as a function of *b*-value proved to be mono-exponential, with no apparent non-Gaussian behavior at least until 1750 s/mm^2 (Fig. S3, S4), in agreement with the behavior expected for self-diffusion in homogeneous liquids [33]. Because high values of T_2 or the ratio T_2/TE can extend the range of linearity to higher *b*-values, it is possible that DWI sequences with shorter TE could expand the range of linearity beyond 2500 s/mm^2 for practical purposes, such as testing kurtosis.

The range of ADC found in this study, especially for concentrations of Ficoll exceeding 20% by weight, overlaps published values for a variety of healthy tissues and tumors [28,34–36].

We challenged the consistency of our results over time and among different scanners, and found good reproducibility, which we attribute to the robustness and versatility of the material and test object. In particular, the stability of Ficoll hydrogels over time is a key feature for use as calibration sample in contexts where ADC may serve as a preclinical or clinical marker. However, for such applications, more work is needed in order to determine additional parameters like the temperature coefficients for due corrections.

Even though our preliminary results show good reproducibility, other solutions like ice-water [6–9,11] and PVP [9,10] are probably even more robust against changing MRI sequence and hardware and environmental temperature fluctuations [6,7]. An ice-water phantom furnished with temperature control [6] showed a variation of measured ADC within 5% with excellent agreement across different systems, and PVP-based phantoms [10] remained below 4% across 13 scanners for a range of diffusivities from 0.4 to 1.1 × 10^{-6} mm^2/s. Phantoms with stabilized temperature are more reliable in multicenter trials, but room temperature alternatives are best suited for everyday purposes like quality control and performance assessment.

In our study, we ascribe the subtle differences in ADC observed across scanners to temperature variations that are not stabilized in this version of the phantom during the measurement session. The effect of temperature on ADC is well known [28,37,38]. Taking into account that the sensitivity of ADC to temperature is about 2.5%/°C in water and between 1.7 and 3.2%/°C in other fluids near room temperature [6–8], we estimate a contribution to the error of ADC around 6%, in our case. To improve the stability and reproducibility of these measurements, the optimization of temperature control within each session and the

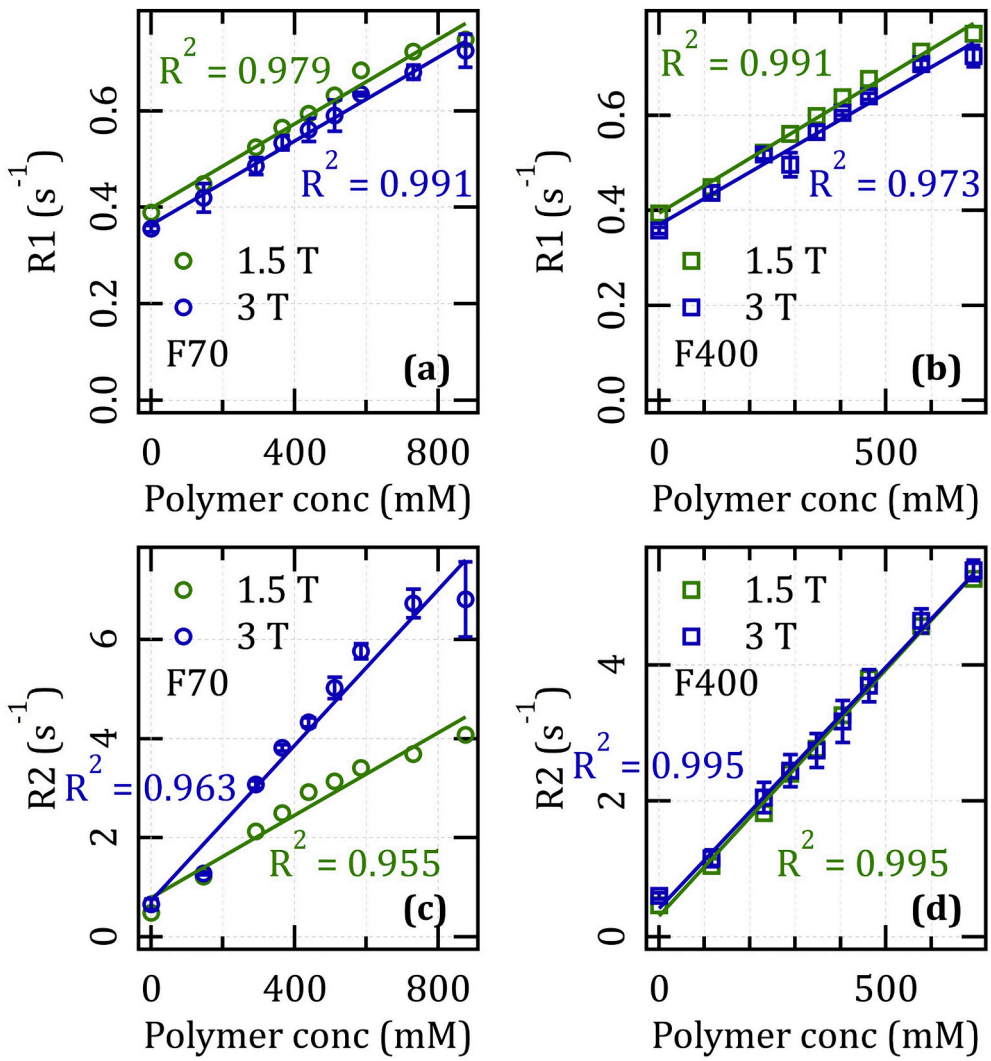

Fig. 4. Results for the R_1 and R_2 relaxation rates measured as a function of Ficoll concentration at 1.5 and 3 T. The linear regression returned R1 = $4.37 \cdot 10^{-4}$ $s^{-1} \cdot mM^{-1}$ · conc $+3.98 \cdot 10^{-1}$ s^{-1} for 1.5 T and R1 = $4.34 \cdot 10^{-4}$ $s^{-1} \cdot mM^{-1}$ · conc $+3.64 \cdot 10^{-1}$ s^{-1} for 3 T in panel a), R1 = $5.76 \cdot 10^{-4}$ $s^{-1} \cdot mM^{-1}$ · conc $+3.94 \cdot 10^{-1}$ s^{-1} for 1.5 T and R1 = $5.53 \cdot 10^{-4}$ $s^{-1} \cdot mM^{-1}$ · conc $+3.70 \cdot 10^{-1}$ s^{-1} for 3 T in panel b), R2 = $4.2 \cdot 10^{-3}$ $s^{-1} \cdot mM^{-1}$ · conc $+7.96 \cdot 10^{-1}$ s^{-1} for 1.5 T and R2 = $7.9 \cdot 10^{-3}$ $s^{-1} \cdot mM^{-1}$ · conc $+7.28 \cdot 10^{-1}$ s^{-1} for 3 T in panel c), and R2 = $7.2 \cdot 10^{-3}$ $s^{-1} \cdot mM^{-1}$ · conc $+3.12 \cdot 10^{-1}$ s^{-1} for 1.5 T and R2 = $7.1 \cdot 10^{-3}$ $s^{-1} \cdot mM^{-1}$ · conc $+4.21 \cdot 10^{-1}$ s^{-1} for 3 T in panel d).

quantification of the sensitivity of ADC to temperature in our samples will be addressed in future studies. In addition, we expect that testing among more scanners will improve the statistics of the measurement.

In addition to their ADC, our preliminary results show the compatibility of the relaxation times of Ficoll hydrogels, especially at polymer concentrations above 20% by weight, with biological tissues like fat, bone marrow, gray matter or muscle [28,34–36,39–41]. A comprehensive study of the relaxation parameters falls outside of the scope of this paper, and further work is needed for their thorough characterization. However, due to their high porosity and density of hydroxyl groups [14,32], we believe that the relaxation processes could be dominated by hydrogen bonding between Ficoll macromolecules and water, as it happens in agar hydrogels [31]. Shortening of the relaxation times, especially of T_1, could be achieved by adding paramagnetic materials like $GdCl_3$ or $NiCl_2$. Together with increasing Ficoll concentration [42] to tune the ADC, this strategy may convey high conformity to a broad variety of human tissues.

The performance of Ficoll 70 and 400 were similar at both 1.5 and 3 T, both polymers providing comparable SNR and behavior of ADC and T_1 as a function of concentration. Only T_2 values seemed to be slightly different between the two, which will require further investigation for an exhaustive explanation.

Using MRI scanners from different vendors, we are bound to use different measurement protocols, probably to the detriment of reproducibility. However, despite this limitation, our experimental conditions are closer to real clinical requirements in view of translational tests.

5. Conclusions

The combination of the physical properties of Ficoll and the design of a phantom container able to accommodate a relevant number of vials allows checking the MRI-DWI operation of commercial clinical scanners with high throughput and consistency. Owing to their tunability, ease of preparation and stability, aqueous solutions of Ficoll represent a potential alternative to other hydrogels in common use, such as agar and agarose, for the setup of MRI phantoms. The ADC values detected for Ficoll 70 and 400 at 1.5 and 3 T were found to range between 0.00125 and 0.00223 mm^2/s and to decrease with polymer concentration. By dosing Ficoll within a relevant phantom design, it is possible to realize quantitative MRI phantoms with tissue-mimicking contrast parameters.

Future work will address the effect of varying the composition of the gel by including additional functional components as well as the consolidation and standardization of the protocols for distribution to the community.

Declaration of Competing Interest

The authors have no conflict of interest to report.

Acknowledgements

We wish to thank Fondazione Toscana "Gabriele Monasterio", Santa Maria Nuova Hospital and Careggi University General Hospital for the use of their MRI clinical facilities, Franco Cosi and Andrea Donati from IFAC-CNR for helping in the realization of the phantom and Roberto Incalcaterra from Santa Maria Nuova Hospital for technical support. FP wishes to thank Anand Yethiraj (Memorial University, Canada) for useful discussions.

Appendix A. Supplementary data

Supplementary data to this article can be found online at https://doi.org/10.1016/j.mri.2020.11.001.

References

[1] Padhani AR, Liu G, Koh DM, Chenevert TL, Thoeny HC, Takahara T, et al. Diffusion-weighted magnetic resonance imaging as a cancer biomarker: consensus and recommendations. Neoplasia. 2009;11(2):102–25. https://doi.org/10.1593/neo.81328.

[2] Tofts PS, Lloyd D, Clark CA, Barker GJ, Parker GJM, McConville P, et al. Test liquids for quantitative MRI measurements of self-diffusion coefficient in vivo. MagnReson Med 2000;43(3):368–74. https://doi.org/10.1002/(SICI)1522-2594(200003)43:3<368::AID-MRM8>3.0.CO;2-B.

[3] Laubach HJ, Jacob PM, Loevbald KO, et al. A phantom for diffusion weighted imaging of acute stroke. J MagnReson Imaging 1998;8:1349–54. https://doi.org/10.1002/jmri.1880080627.

[4] Russek SE, Boss M, Jackson EF, et al. Characterization of NIST/ISMRM MRI system phantom. Proc Int Soc Magn Reson Med 2012;22:2456.

[5] Hellerbach A, Schuster V, Jansen A, Sommer J. MRI Phantoms – Are There Alternatives to Agar? PLoSONE 2013;8(8). https://doi.org/10.1371/journal.pone.0070343. e70343.

[6] Chenevert TL, et al. Diffusion coefficient measurement using a temperature-controlled fluid for quality control in multicenter studies. J Magn Reson Imaging 2011;34:983–7. https://doi.org/10.1002/jmri.22363.

[7] Malyarenko D, et al. Multi-system repeatability and reproducibility of apparent diffusion coefficient measurement using an ice-water phantom. J Magn Reson Imaging 2013;37:1238–46. https://doi.org/10.1002/jmri.23825.

[8] Moreau B, et al. EurRadiol 2018;28:3362. https://doi.org/10.1007/s00330-017-5265-2.

[9] Keenan KE, et al. Recommendations towards standards for quantitative MRI (qMRI) and outstanding needs. J Magn Reson Imaging 2019;49:e26–39. https://doi.org/10.1002/jmri.26598.

[10] Mulkern RV, et al. Pediatric brain tumor consortium multisite assessment of apparent diffusion coefficient z-axis variation assessed with an ice–water phantom. Acad Radiol 2015;22(3). https://doi.org/10.1016/j.acra.2014.10.006.

[11] Palacios EM, et al. Am J Neuroradiol 2017;38(3):537–45. https://doi.org/10.3174/ajnr.A5025.

[12] Keenan KE, et al. Quantitative magnetic resonance imaging phantoms: a review and the need for a system phantom. Magn Reson Med 2018;79:48–61. https://doi.org/10.1002/mrm.26982.

[13] https://www.gelifesciences.co.jp/catalog/pdf/18115827.pdf. Accessed May 22, 2019.

[14] Palit S, Yethiraj A. Dynamics and cluster formation in charged and uncharged Ficoll70 solutions. J Chem Phys 2017;147(7):074901. https://doi.org/10.1063/1.4986366.

[15] Fissell WH, Hofmann CL, Smith R, Chen MH. Size and conformation of Ficoll as determined by size-exclusion chromatography followed by multiangle light scattering. Am J Physiol Renal Physiol 2010;298(1):F205–8. https://doi.org/10.1152/ajprenal.00312.2009.

[16] Tokuriki N, Kinjo M, Negi S, et al. Protein folding by the effect of macromolecular crowding. Protein Sci 2004;13(1):125–33. https://doi.org/10.1110/ps.03288104.

[17] Bhattacharya A, Kim YC, Mittal J. Protein-protein interactions in a crowded environment. Biophys Rev 2013;5(2):99–108. https://doi.org/10.1007/s12551-013-0111-5.

[18] Baumann P, Spulber M, Fischer O, Car A, Meier W. Investigation of horseradish peroxidase kinetics in an "organelle-like". Environ Small 2017;13(17):1603943. https://doi.org/10.1002/smll.201603943.

[19] Vöpel T, Makhatadze GI. Enzyme activity in the crowded milieu. PLoS One 2012;7(6):e39418. https://doi.org/10.1371/journal.pone.0039418.

[20] Georgalis Y, Philipp M, Aleksandrova R, Krüger JK. Light scattering studies on Ficoll PM70 solutions reveal two distinct diffusive modes. J Colloid Interface Sci 2012;386(1):141–7. https://doi.org/10.1016/j.jcis.2012.07.062.

[21] Dauty E, Verkman AS. Molecular crowding reduces to a similar extent the diffusion of small solutes and macromolecules: measurement by fluorescence correlation spectroscopy. J MolRecognit 2004;17(5):441–7. https://doi.org/10.1002/jmr.709.

[22] Luby-Phelps K. Cytoarchitecture and physical properties of cytoplasm: volume, viscosity, diffusion, intracellular surface area. Int Rev Cytol 2000;192:189–221. https://doi.org/10.1016/S0074-7696(08)60527-6.

[23] Wong KHK, Sandlin RD, Carey TR, et al. The role of physical stabilization in whole blood preservation. Nat Sci Rep 2016;6:21023. https://doi.org/10.1038/srep21023.

[24] Deen WM, Lazzara MJ, Myers BD. Structural determinants of glomerular permeability. Am J Physiol Renal Physiol 2001;281:F579–96. https://doi.org/10.1152/ajprenal.2001.281.4.F579.

[25] Barucci A, Belli G, Carpi R, et al. A phantom for temperature monitoring in hyperthermia therapy with gold nanoparticles using magnetic resonance imaging. IET Conference Proceedings 2018. https://doi.org/10.1049/cp.2018.1669.

[26] Report of the Italian Association of Medical Physics (AIFM) n. 12. Assicurazione di qualità in DWI; 2016. ISBN 978–88–907973-6-1.

[27] Dietrich O, Raya JG, Reeder SB, Reiser MF, Schoenberg SO. Measurement of signal-to-noise ratios in MR Images: influence of multichannel coils, parallel imaging, and reconstruction filters. JMagnResonIm. 2007;26:375–85.

[28] Hara M, Kuroda M, Ohmura Y, et al. A new phantom and empirical formula for apparent diffusion coefficient measurement by a 3 tesla magnetic resonance imaging scanner. OncolLett. 2014;8(2):819–24. https://doi.org/10.3892/ol.2014.2187.

[29] Schneider CA, Rasband WS, Eliceiri KW. NIH Image to ImageJ: 25 years of image analysis. Nat Methods 2012;9(7):671–5. PMID 22930834.

[30] Le Bihan D, Poupon C, Amadon A, Lethimonnier F. Artifacts and Pitfalls in Diffusion MRI. J.Magn.Reson.Im. 2006;24:478–88. https://doi.org/10.1002/jmri.20683.

[31] Davies E, Huang Y, Harper JB, Hook JM, Thomas DS, Burgar IM, et al. Dynamics of water in agar gels studied using low and high resolution 1H NMR spectroscopy. Int J Food Sci Technol 2010;45:2502–7. https://doi.org/10.1111/j.1365-2621.2010.02448.x.

[32] Aouissi Z, Mahjoub HF, Aschi A, Othman T. Temperature study of Ficoll400 aqueous solutions, evidence of bad solvent around 35 °C. J Mol Liq 2017;241:435–46. https://doi.org/10.1016/j.molliq.2017.06.030.

[33] Jensen JH, Helpern JA. MRI quantification of Non-Gaussian water diffusion by kurtosis analysis. NMR Biomed 2010;23(7):698–710. https://doi.org/10.1002/nbm.1518.

[34] Hambrock T, Somford DM, Huisman HJ, et al. Relationship between apparent diffusion coefficients at 3.0-T MR imaging and Gleason grade in peripheral zone prostate cancer. Radiology. 2011;259(2):453–61. https://doi.org/10.1148/radiol.11091409.

[35] Taouli B, Koh DM. Diffusion-weighted MR imaging of the liver. Radiology. 2010;254(1):47–66. https://doi.org/10.1148/radiol.09090021.

[36] Tan SL, Rahmat K, Rozalli FI, et al. Differentiation between benign and malignant breast lesions using quantitative diffusion-weighted sequence on 3 T MRI. ClinRadiol. 2014;69(1):63–71. https://doi.org/10.1016/j.crad.2013.08.007.

[37] Holz M, Heil SR, Sacco A. Temperature-dependent self-diffusion coefficients of water and six selected molecular liquids for calibration in accurate ^{1}H NMR PFG measurements. Phys Chem Chem Phys 2000;2:4740–2.

[38] Matsuya R, Kuroda M, Matsumoto Y, Kato H, Matsuzaki H, Asaumi J. A new phantom using polyethylene glycol as an apparent diffusion coefficient standard for MR imaging. Int J Oncol 2009;35:893–900. https://doi.org/10.3892/ijo_00000404.

[39] Bojorquez JZ, Bricq S, Acquitter C, Brunotte F, Walker PM, Lalande A. What are normal relaxation times oftissues at 3 T? MagnResonIm. 2017;35:69–80. https://doi.org/10.1016/j.mri.2016.08.021.

[40] Wansapura JP, Holland SK, Dunn RS, Ball Jr WS. NMR relaxation times in the human brain at 3.0 tesla. JMagnReson Im 1999;9(4):531–8. doi: 10.1002/(SICI)1522-2586(199904)9:4<531::AID-JMRI4>3.0.CO;2-L.

[41] Gold GE, Han E, Stainsby J, Wright G, Brittain J, Beaulieu C, et al. At 3.0 T: RelaxationTimes and image contrast. AJR Am JRoentgenol 2004;183(2):343–51. https://doi.org/10.2214/ajr.183.2.1830343.

[42] Kato H, Kuroda M, Yoshimura K, et al. Composition of MRI phantom equivalent to human tissues. Med Phys 2005;32(10):3199–208. https://doi.org/10.1118/1.2047807.